

# Orbital-optimized pair-correlated electron simulations on trapped-ion quantum computers

Luning Zhao,<sup>\*</sup> Joshua Goings, Kenneth Wright, Jason Nguyen, Jungsang Kim, and Sonika Johri  
*IonQ Inc, College Park, MD, 20740, USA*

Kyujin Shin<sup>†</sup> and Woomin Kyoung  
*Materials Research & Engineering Center, R&D Division,  
Hyundai Motor Company, Uiwang 16082, Republic of Korea*

Johanna I. Fuks  
*Qunova Computing, Daejeon, 34051, Republic of Korea*

June-Koo Kevin Rhee  
*Qunova Computing, Daejeon, 34051, Republic of Korea and  
School of Electrical Engineering, KAIST, Daejeon, 34141, Republic of Korea*

Young Min Rhee  
*Department of Chemistry, KAIST, Daejeon, 34141, Republic of Korea*  
(Dated: December 6, 2022)

Variational quantum eigensolvers (VQE) are among the most promising approaches for solving electronic structure problems on near-term quantum computers. A critical challenge for VQE in practice is that one needs to strike a balance between the expressivity of the VQE ansatz versus the number of quantum gates required to implement the ansatz, given the reality of noisy quantum operations on near-term quantum computers. In this work, we consider an orbital-optimized pair-correlated approximation to the unitary coupled cluster with singles and doubles (uCCSD) ansatz and report a highly efficient quantum circuit implementation for trapped-ion architectures. We show that orbital optimization can recover significant additional electron correlation energy without sacrificing efficiency through measurements of low-order reduced density matrices (RDMs). In the dissociation of small molecules, the method gives qualitatively accurate predictions in the strongly-correlated regime when running on noise-free quantum simulators. On IonQ's Harmony and Aria trapped-ion quantum computers, we run end-to-end VQE algorithms with up to 12 qubits and 72 variational parameters - the largest full VQE simulation with a correlated wave function on quantum hardware. We find that even without error mitigation techniques, the predicted relative energies across different molecular geometries are in excellent agreement with noise-free simulators.

## I. INTRODUCTION

Finding accurate solutions to the electronic structure problem is of great importance to various industries, from modeling pharmaceutical drug docking [1], to designing new materials for light harvesting and CO<sub>2</sub> reduction [2], to elucidating reaction mechanisms in novel battery materials [3]. However, the classical computational resources needed to solve the electronic structure problem exactly scales exponentially with the size of systems, which limits routine or practical application to systems with less than 20 electrons. To make the problem tractable on classical computers, various approximate approaches have been developed, each with different trade-offs between cost and accuracy. These approaches include density functional theory (DFT)[4], coupled cluster (CC)[5] methods, density matrix renormalization group methods (DMRG)[6], and quantum Monte Carlo methods (QMC)[7]. These methods are routinely applied toward computational chemistry calculations both in academia and in industry.

Despite the abundance of different classical approxima-

tions, the electronic structure problem is far from being solved. For example, systems with strongly correlated electronic structure are notoriously difficult to solve. These systems are commonly encountered during bond breaking and formation, as well as when studying systems such as transition-metal-containing catalysts, large  $\pi$ -conjugated systems, and high-temperature superconductors. In these cases, approximate approaches may either fail completely (such as in single-reference methods like DFT or CC), or will be prohibitively costly (such as in multi-reference methods like DMRG or QMC). It is possible that approximate classical approaches will never reliably solve the strong correlation problem.

In contrast, quantum computation[8] has attracted significant attention for its potential to solve certain computational problems more efficiently than with classical computers, especially since IBM launched the first cloud accessible quantum computer and Google demonstrated quantum advantage[9]. One of its most promising applications is to solve electronic structure problems efficiently[10]: to illustrate, consider that for a problem containing  $N$  spin orbitals, the number of classical bits required to represent the wave function scales combinatorially with  $N$ , while on a quantum computer only  $N$  qubits are needed. The exponential advantage offered by quantum computers has motivated a great deal of research in developing quantum algorithms to solve the

<sup>\*</sup> zhao@ionq.co

<sup>†</sup> shinkj@hyundai.com

electronic structure problem.

Of these, the variational quantum eigensolver (VQE) algorithm [11–15] is designed specifically for current near-term intermediate scale quantum (NISQ) computers. VQE estimates the ground state of a system by implementing a shallow parameterized circuit, which is classically optimized to variationally minimize the energy expectation value. The VQE algorithm allows the user to select the form of the parameterized circuit. This flexibility allows one to adjust the circuit depth based on the quantum gate fidelity, number of qubits, and desired accuracy. This makes VQE especially suitable for the NISQ era.

There is, however, no free lunch and the ability to run shallower circuits within the VQE comes with two costs. First, the predicted energy in most cases remains approximate, because the accuracy depends on the expressivity of the circuit form. Second, one needs to perform a large number of measurements for VQE. This makes the choice of the ansatz perhaps the most important building block in the VQE algorithm. So what does one choose? Early demonstrations of VQE on quantum hardware utilized the physically-motivated unitary coupled cluster with singles and doubles (uCCSD) ansatz [16, 17]. uCCSD is well-known in the quantum chemistry community to be able to treat strongly correlated systems, while remaining classically intractable. As such, A. Peruzzo *et al.* [11] used the uCCSD ansatz in the first VQE demonstration on a photonic quantum computer to solve for the  $H_2$  molecule in a minimal basis. O’Malley and coworkers [12] performed the same simulations on a superconducting quantum computer with two qubits. In 2019, McCaskey [18] and co-workers simulated metal hydrides in a 2-electron, 2-orbital active space using the uCCSD ansatz on IBM’s superconducting quantum computers with four qubits. However, going beyond a minimal active space poses difficulties due to the rapid increase in the number of entangling gates for the uCCSD ansatz. The number of entangling gates in uCCSD (e.g. *CNOT*) scales as  $O(N^4)$ , where  $N$  is the number of qubits. Even the most efficient implementation of uCCSD circuits contain thousands of entangling gates for small systems [19], which makes it impractical to run on NISQ quantum computers.

Due to the impracticality of the uCCSD ansatz on NISQ quantum computers, hardware efficient ansatzes (HEA) [13, 20–23] have attracted significant attention. Compared to the uCCSD ansatz, HEAs need significantly shallower circuits. In 2017, researchers from IBM published the first study [13] of using HEAs on superconducting quantum computers to simulate  $H_2$ ,  $LiH$ , and  $BeH_2$  with 2, 4, and 6 qubits. However, noise in the quantum processing unit (QPU) led to unphysical behavior in the predicted dissociation curve. In 2019, the same researchers [24] use HEAs to demonstrate quantum error mitigation using the zero-noise extrapolation technique with 4 qubits. In 2021, researchers [25] used HEAs to study thermally activated delayed fluorescence (TADF) with 2 qubits on superconducting quantum computers. They found that without using an unscalable error mitigation approach, even a 2-qubit circuit yields qualitatively inaccurate predictions to the relative energy.

The largest VQE simulation performed on quantum hard-

ware so far is the Hartree-Fock (HF) study by Google [14], in which they used a superconducting quantum computer to simulate the HF wave function for hydrogen chains up to 12 qubits and 72 entangling gates. However, the calculations faced a considerable amount of hardware noise, necessitating the use of Hartree-Fock specific error mitigation techniques to achieve sufficiently accurate results. A more recent study by Google [26] simulated a cyclobutene ring on a superconducting quantum computer with up to 10 qubits using pair-correlated wave functions. Here, the ansatz was classically pre-optimized on a simulator, leaving the final energy evaluation to be executed on the quantum device. Despite this, this calculation still required classical error mitigation techniques to achieve reasonable results for the final quantum energy evaluation.

Trapped-ion quantum computers have several unique advantages over other currently available quantum computing architectures. First, the gate fidelity for trapped-ion qubits is typically higher than for superconducting qubits, which enables users to run deeper circuits. Second, trapped-ion qubits are all-to-all connected. This means one is able to entangle arbitrary pairs of qubits without performing expensive *SWAP* operations to entangle non-adjacent qubits, which is usually required on systems with interactions that do not form a complete graph. Although both of these advantages should lead to higher fidelity when running VQE circuits, implementations of VQE on trapped-ion quantum computers are rare, and this is mainly due to comparatively limited availability of the trapped ion quantum computing hardware versus superconducting quantum computers. In this work, we fill this gap by performing VQE simulations on two generations of trapped-ion quantum computers constructed by IonQ, Inc.

We consider an approximate ansatz derived from the uCCSD ansatz: the unitary pair CCD (upCCD) ansatz, in which only paired double excitations are retained. This allows us to map the fermionic representation to electron pairs, known as the hard-core boson representation. From this, we show that the unitary pCCD ansatz then requires half the number of qubits to encode the state vector as compared to the uCCSD ansatz. We then introduce the optimal circuit for implementing an arbitrary electron pair excitation in terms of the number of *CX* gates. The energy expression for the upCCD ansatz is derived, and we find that at most 3 circuits are needed to compute the energy expectation value, regardless of the size of the system. The shallow circuit structure, along with a constant low number of measurements required, make the upCCD ansatz a perfect candidate on NISQ quantum computers.

The accuracy of the upCCD ansatz depends on the choice of the underlying orbitals. Previous studies on similar wave functions have found that it is necessary to optimize the orbitals along with the cluster amplitudes, especially for strongly correlated systems. In this work, we find that the orbital optimization effects can be incorporated through classical post-processing, and only requires the measurements of one- and two-body reduced density matrices (RDM) of the upCCD ansatz on the quantum device. In our experiments, we observe that failure to use orbital optimization results in highly non-physical energy predictions in the bond-

dissociation regime, but physical behavior can be fully recovered by optimizing orbitals together with parameters in the upCCD ansatz. Due to the symmetry of the upCCD ansatz, the energy measurements automatically yield the required measurements for RDMs. This allows us to improve the expressivity of the ansatz, especially for strongly correlated systems without increasing the circuit depth on the quantum computer.

In Table I, we list a collection of techniques used in the study, with inventions in this work marked in *italic*. Our result (see Table II) is the largest full VQE demonstration on a QPU using a correlated wave function without error mitigation.

The paper is structured as follows. We begin by introducing the upCCD ansatz, then discuss the mapping from electron pairs to Pauli matrices, and an efficient quantum circuit implementation of the ansatz. We then derive the energy expression for the upCCD ansatz. Having laid out the general formalism, we then introduce the orbital optimization of upCCD using RDMs and the Newton-Raphson algorithm. Results are presented on quantum simulators and IonQ’s Harmony and Aria quantum computers for potential energy surface predictions of LiH, H<sub>2</sub>O, and Li<sub>2</sub>O molecule. All the VQE experiments on simulator and quantum computers are end-to-end VQE runs, which means we perform both parameter optimizations and final energy evaluations. We conclude with a summary of our findings and comments on future directions.

Readers are strongly encouraged to read “Methods” section before “Results” section. In “Methods” section, we describe the details of the quantum computer hardware used to run VQE and the specifics of the molecular models used to generate the quantum simulation circuits. We heavily use the notations defined in “Methods” section throughout “Results” section.

## II. RESULTS

### A. The VQE Algorithm and Circuit

The unitary pair Coupled Cluster double (upCCD) ansatz is

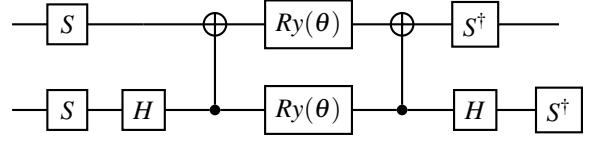
$$|\Psi_{\text{upCCD}}\rangle = e^{T-T^\dagger} |\text{HF}\rangle \quad (1)$$

in which  $T$  is the pair-double cluster operator, defined as

$$T = \sum_{ia} t_i^a a_{a\alpha}^\dagger a_{a\beta}^\dagger a_{i\beta} a_{i\alpha} \quad (2)$$

in which  $i$  and  $a$  are indices for occupied and unoccupied orbitals in the HF state.  $a_{p\alpha}^\dagger$  ( $a_{p\beta}^\dagger$ ) and  $a_{p\alpha}$  ( $a_{p\beta}$ ) are the Fermionic creation and annihilation operators in the  $p$ th spin up (down) orbital.

Each exponentiation of the pair-excitation operator can be efficiently implemented with the following circuit,



Once the circuit is defined, one needs to measure the energy expectation value  $\langle \Psi_{\text{upCCD}} | H | \Psi_{\text{upCCD}} \rangle$  for the second-quantized Hamiltonian  $H$ . Originally, there are  $O(N^4)$  terms in  $H$ , in which  $N$  is the number of qubits. However, a majority of them do not contribute to the energy since they break pair symmetry. After eliminating these terms, one finds that only 3 measurements are needed in the  $X$ ,  $Y$ , and  $Z$  basis respectively to compute the energy, regardless of the system size.

The upCCD ansatz defined in Equation 1 is not invariant to the choice of underlying orbitals. Previous studies [39–42] on similar wave functions have found that it is necessary to optimize the orbitals along with the cluster amplitudes, especially for strongly correlated systems. The orbital optimized upCCD ansatz is

$$|\Psi_{\text{oo-upCCD}}\rangle = e^K e^{T-T^\dagger} |\text{HF}\rangle \quad (3)$$

in which there are two different sets of parameters: 1) circuit parameters in the cluster operator  $T$ ; 2) orbital rotation parameters in the the orbital rotation operator  $K$ , which is defined as

$$K = \sum_{p>q} \sum_{\sigma} K_{pq} (a_{p\sigma}^\dagger a_{q\sigma} - a_{q\sigma}^\dagger a_{p\sigma}) \quad (4)$$

where  $K$  is an anti-Hermitian matrix and  $\sigma$  indexes the spin.

As shown in the Methods section, we find the optimal set of orbital rotation parameters  $K_{pq}$  with the Newton-Raphson (NR) algorithm, in which the energy gradient and Hessian are measured on the quantum computer. Then, the effect of orbital rotation operators can be fully absorbed into one- and two-electron integrals through integral transformation, which is done efficiently on classical computers. In this way doing orbital optimization does not increase the circuit depth or the number of measurements.

### B. Experimental Example

All the calculations and experiments were performed using IonQ’s in-house quantum chemistry library, which facilitates the preparation and execution of quantum variational algorithms on IonQ’s cloud simulators and QPUs. We used the PySCF [43] software suite to compute the molecular integrals necessary to define the second-quantized Hamiltonian, as well as compute the classical FCI reference energies.

#### 1. LiH

We begin with our bond dissociation results with a simple example, the LiH molecule. The system has only two valence electrons. We freeze the Li 1s orbital, and also exclude the molecular orbitals formed with Li’s 2px and 2py orbitals

TABLE I: Techniques and their corresponding effects used in the paper.

Technique	Effect	Previous work
Electron Pair $\rightarrow$ Bosons	Reduce number of qubits by a factor of 2	[15]
Givens Rotation with Magic Gate	Most efficient Givens rotation implementation in terms of $CX$ gates	[27]
Hamiltonian Grouping	3 circuits per energy measurements regardless of system size	[28]
Measurement of RDMs	3 circuits for all 1- and 2-RDMs regardless of system size	this work
Orbital Optimization with Newton-Raphson	Increase circuit expressivity without increasing depth	this work

TABLE II: Comparison between this work and previous publicly-reported VQE chemistry simulations on QPUs.

Year	Ansatz	System	# Qubits	# Parameters	Full VQE?	Error Mitigation?	Hardware Vendor
2022	oo-upCCD [this work]	Li <sub>2</sub> O	12	72	Yes	No	IonQ
2022	upCCD [26]	Cyclobutene Ring	10	25	No	Yes	Google
2022	uCCSD [29]	CH <sub>3</sub>	6	4	No	Yes	Quantinuum
2022	YXXX [30]	oxazine derivatives	4	1	Yes (superconducting), No (trapped-ion)	Yes	IBM, Quantinuum
2022	uCCSD-PBC [31]	crystalline iron model	2	1	Yes	Yes	IBM
2022	Entang. Forging [32]	H <sub>3</sub> S <sup>+</sup>	6	8	No	Yes	IBM
2022	Entang. Forging [33]	H <sub>2</sub> O	5	3	Yes	Yes	IBM
2021	HEA [3]	LiH (dipole moment)	4	16	Yes	Yes	IBM
2021	HEA [25]	TADF	2	4	Yes	Yes	IBM
2021	qubit CC [34]	H <sub>10</sub>	2	3	No	Yes	IonQ
2021	HEA [35]	Li <sub>2</sub> O <sub>4</sub> model	2	4	Yes	Yes	IBM
2020	Hartree-Fock [14]	H <sub>12</sub>	12	36	Yes	Yes	Google
2020	upCCD [15]	H <sub>2</sub> O	3	3	Yes	No	IonQ
2019	HEA [24]	LiH	4	20	Yes	Yes	IBM
2019	reduced uCC [36]	NaH, KH, RbH	4	3	No	Yes	IBM, Rigetti
2018	uCCSD [37]	H <sub>2</sub> (excited states)	2	1	Yes	No	UCB, LBNL
2017	HEA [13]	BeH <sub>2</sub>	6	30	Yes	No	IBM
2016	uCCSD [12]	H <sub>2</sub>	2	1	No (scan)	No	UCSB
2014	uCCSD [38]	HeH <sup>+</sup>	2	6	Yes	No	Univ. of Bristol

since they do not contribute to the correlation energy due to symmetry. By doing so we only need 3 qubits and the VQE circuits consists of only 4  $CX$  gates. In Figure 1, we compare the energy predicted by FCI, upCCD, and oo-upCCD. As shown in the plot, both upCCD and oo-upCCD result in accurate energy predictions when the molecule is in the equilibrium geometry. However, as we enter the stretched region, upCCD gives highly nonphysical predictions. Not only does the energy error increases to tens of millihartrees, but it also exhibits a ‘‘hump’’ in the potential energy surface (PES). Such a nonphysical behavior is primarily due to the break down of the mean-field picture in stretched geometries. To the contrary, the oo-upCCD energy prediction matches FCI in both equilibrium and the stretched regions, which demonstrates the importance of orbital optimization.

We then move from simulators to quantum hardware. In Figure 2, we show the results obtained from IonQ’s Harmony quantum computer. The system has 11 all-to-all connected qubits, and the averaged single and two-qubit gate fidelities are 99% and 98%. It has been used in numerous applications, including quantum chemistry [15, 34], quantum machine learning [44, 45], and finance [46, 47]. Due to the limited machine time, instead of scanning the entire PES, we selected a few points from squeezed, equilibrium, and stretched geometries. As shown in the plot, the energy measured on noisy quantum hardware is much higher than the

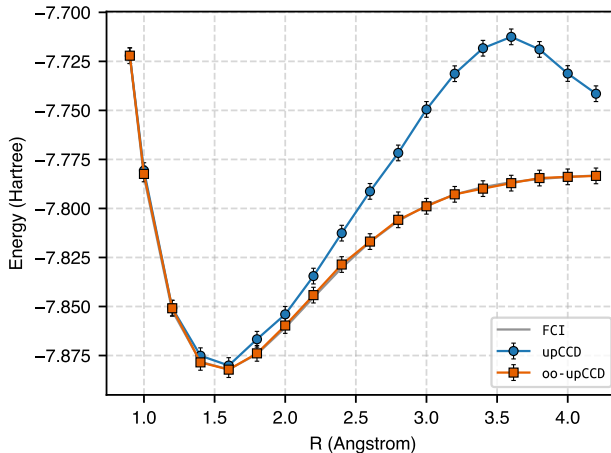


FIG. 1: Dissociation of LiH in STO-3G basis set comparing upCCD, oo-upCCD, and FCI. VQE results are obtained from a noise-free quantum simulator.

simulation results. However, we also find that the amount of error is consistent along the PES. Based on such an observation, we shifted all the measured energies so that the energy at  $R = 1.6$  Angstrom matches the simulation energy. By do-

ing so, the shifted energies matches well with the exact energy. This is notable especially with the stretched geometry  $R = 3.0$  Angstrom, in which the shifted energy falls on the simulated PES of oo-upCCD, demonstrating that the orbital optimization effects are successfully captured by the quantum hardware.

Lastly, we ran the same simulation on IonQ Aria: IonQ’s latest generation quantum computer and the results are shown in Figure 2. IonQ Aria offers both more qubits and improved gate fidelities over IonQ Harmony. We find that the improved gate fidelities reduces the amount of error in energy by 38%. Once shifted, the relative energy also matches the exact energy within statistical uncertainty. The improvements from Harmony to Aria are not very large in this case due to the simplicity of the circuit, which contains only 4  $CX$  gates.

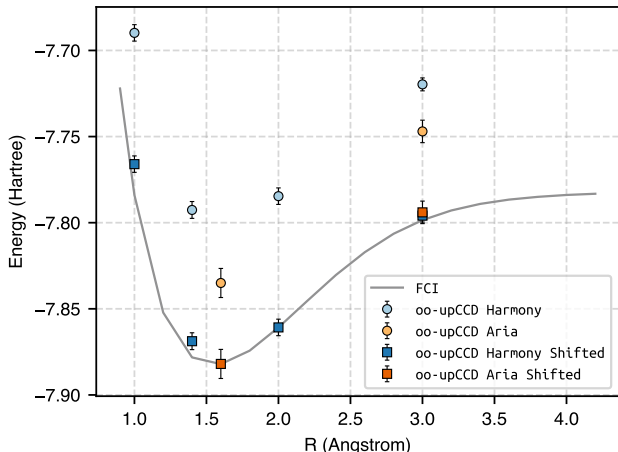


FIG. 2: Dissociation of LiH in STO-3G basis set comparing upCCD, oo-upCCD, and FCI. VQE results are obtained from the IonQ Harmony and the IonQ Aria quantum computer.

## 2. $H_2O$

Our next example is the symmetric double dissociation of  $H_2O$ , as shown in Figure 3 for results obtained on the simulator. We only freeze the O 1s core orbital and keep all other orbitals in the active space. The total number of qubits required is 6 and there are 16  $CX$  gates in the circuit. Again, oo-upCCD produces highly accurate energies compared with FCI. However, unlike LiH, in which oo-upCCD matches FCI exactly, in  $H_2O$  we find the predicted energy error for oo-upCCD is about 20 millihartrees, especially when we are in the stretched geometry. The error is due to the omission of the un-paired excitations in the oo-upCCD ansatz. However, we also note that without orbital optimization, the upCCD ansatz using the HF orbitals yields more than 200 millihartrees of error in energy, again emphasizing the importance of orbital optimization.

Before running the circuit on quantum hardware, we first remove redundant parameters from the ansatz. The redundant parameters are the circuit parameters that do not contribute

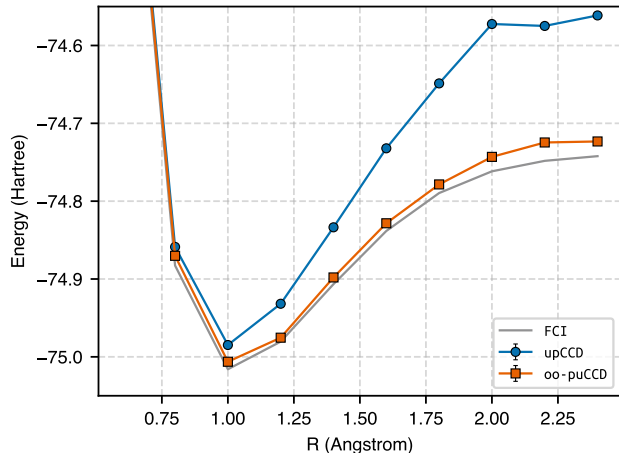


FIG. 3: Dissociation of  $H_2O$  in STO-3G basis set comparing upCCD, oo-upCCD, and FCI. VQE results are obtained from a noise-free quantum simulator. The statistical error from the 6000 shots is not visible at this scale.

to the energy, and their amplitudes stay zero during the optimization process. For the  $H_2O$  molecule, an example of redundant parameters are the amplitudes that correspond to pair excitations from the non-bonding orbital. In this study, we identify redundant parameters by tracking the evolutions of parameter amplitudes on a noise-free simulator, with all parameters started from zero. Parameters whose amplitudes stay at zero during the entire optimization process are identified as redundant parameters. It is worth noting that such an approach does not scale as the system size, and the running time on simulator becomes prohibitively expensive. Fortunately, there exist scalable approaches for identifying and simulating only non-redundant parameters, such as the gradient based selection used for the ADAPT-VQE[17] method.

Upon removal of redundant parameters, we are able to reduce the circuit to contain 4 circuit parameters and 8  $CX$  gates. We then performed the oo-upCCD simulation on IonQ’s Aria quantum computer, and the results are shown in Figure 4. The simulation is done on two geometry points: one at the equilibrium geometry and the other one at the stretched geometry. We find that the Aria quantum computer successfully finds the optimal parameters and captures the orbital optimization effects. Similar to LiH, the noise on the hardware introduce a systematic, positive bias to the measured absolute energy, but such a bias is constant at different geometry points. Once we shift the absolute energies by a constant, the energies match the ones measured on a noise-free simulator, which demonstrates that the hardware noise is consistent enough so that the predicted relative energies are accurate.

## 3. $Li_2O$

Our final example is the symmetric dissociation of the  $Li_2O$  molecule.  $Li_2O$  is one of the secondary reaction products in lithium-air batteries, which is believed to be a candidate for next-generation lithium battery due to its high energy den-

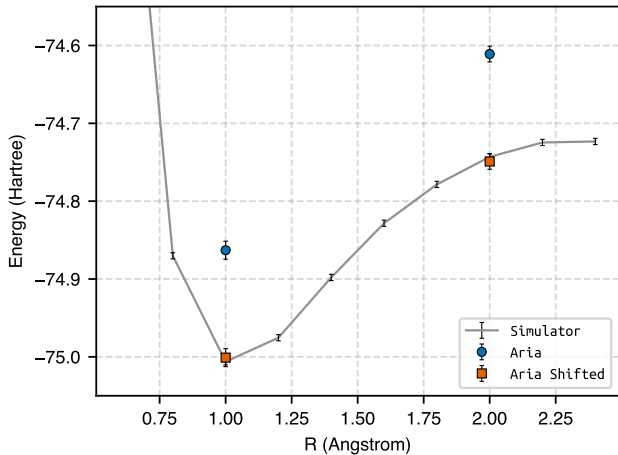


FIG. 4: Dissociation of  $\text{H}_2\text{O}$  in STO-3G basis set comparing oo-upCCD VQE results obtained from the IonQ Aria quantum computer and a noise-free simulator.

sity. We freeze the  $1s$  orbital for Li and O, resulting in a circuit with 12 qubits and 64  $CX$  gates. The results on an ideal simulator are shown in Figure 5. The difference in energy between oo-upCCD and FCI becomes more noticeable, which is expected since  $\text{Li}_2\text{O}$  has twice (four times) the number of orbitals as  $\text{H}_2\text{O}$  ( $\text{LiH}$ ). As a result, there are many more unpaired excited configurations in  $\text{Li}_2\text{O}$  than  $\text{H}_2\text{O}$  and  $\text{LiH}$ , and ignoring them, as is being done in the upCCD ansatz, introduces a more drastic approximation. Again, we find that orbital optimization does not make any noticeable amount of difference in equilibrium geometry, but becomes crucial in stretched geometries.

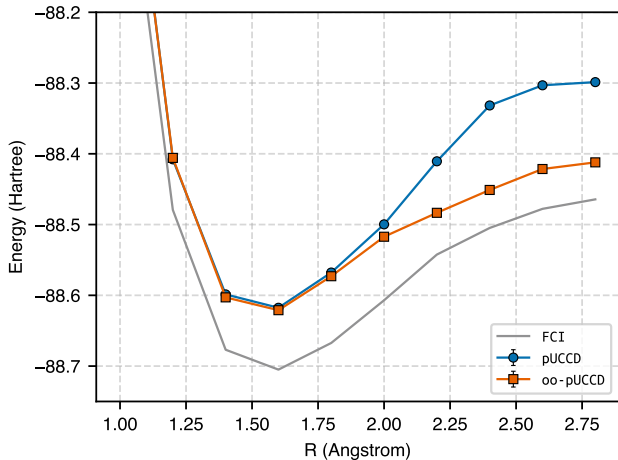


FIG. 5: Dissociation of  $\text{Li}_2\text{O}$  in STO-3G basis set comparing upCCD, oo-upCCD, and FCI. VQE results are obtained from a noise-free quantum simulator. The statistical error from the 6000 shots is not visible at this scale.

We then performed the oo-upCCD simulation on the Aria quantum computer. Analogous to  $\text{H}_2\text{O}$ , we first identify and remove redundant parameters. In this example we find that

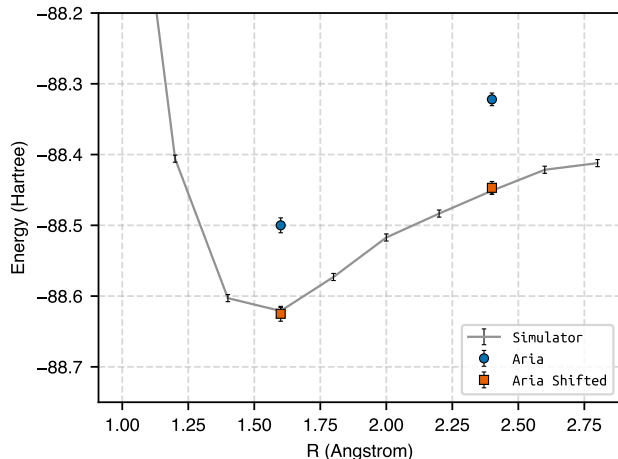


FIG. 6: Dissociation of  $\text{Li}_2\text{O}$  in STO-3G basis set comparing oo-upCCD VQE results obtained from the IonQ Aria quantum computer and a noise-free simulator.

only 6 out of the 32 circuit parameters are non-redundant. Therefore, we only implement and optimize these 6 circuit parameters (12  $CX$  gates) on the quantum hardware, with an additional 66 orbital rotation parameters, for 72 variational parameters total. The results are shown in Figure 6 at two geometry points: one at the equilibrium geometry and another one at the stretched geometry. Like in  $\text{H}_2\text{O}$ , we find that despite hardware noise, the predicted relative energy matches the simulator's prediction, and the orbital optimization effects are successfully captured by Aria.

### III. DISCUSSION

Quantum computers are expected to be able to efficiently solve the electronic structure problem. In principle, the electronic energy can be exactly computed in polynomial time using quantum phase estimation (QPE)[48] or its iterative variant[49]. In contrast, the best equivalent classical algorithm (full configuration interaction, or FCI) scales exponentially. In QPE, one implements the time propagator  $U = \exp(-iHt)$  on the quantum computer and operates it on an efficiently prepared trial state. Assuming the trial state has sufficient overlap with the exact eigenstate  $|\Psi_i\rangle$ , the exact eigenstate's energy is encoded in the phase of the wave function since  $U|\Psi_i\rangle = \exp(-iE_it)|\Psi_i\rangle$ . The phase can be extracted using the quantum Fourier transform (QFT).

While the QPE algorithm can compute the energy levels of molecules exactly, it is impractical on current NISQ computers. In the NISQ era, quantum gates are noisy, and entangling gates are typically an order of magnitude lower in fidelity compared to single qubit gates. This means that one can only perform a limited number of quantum operations to ensure that the results are distinguishable from noise. This poses a significant difficulty for the QPE algorithm, as the implementation of the time propagator is very expensive and yields deep quantum circuits. QPE algorithms without using the time propagator, such as qubitization [50–52] have also been

developed with improved scaling, but the fact remains that neither algorithm results in circuits that are shallow enough to run on quantum computers without error-corrected qubits.

We therefore focus on VQE, an algorithm expressly designed for NISQ computers. Here, we have developed an efficient VQE algorithm that is able to run on near-term quantum computers with high accuracy. The algorithm employs a chemically-inspired ansatz based on the unitary pair coupled cluster doubles (upCCD) wave function. The upCCD ansatz is obtained from the general unitary CCSD ansatz by retaining only paired double excitations. This allows us to condense electron pairs to the hard-core boson representation and develop an efficient quantum circuit implementation that only requires 2  $CX$  gates to implement one excitation. Since the accuracy of the upCCD ansatz depends on the underlying orbital choice, we developed an orbital optimization algorithm that finds the variationally optimal set of orbitals automatically. We find that orbital optimization can be implemented efficiently by measuring one- and two-body RDMs on a quantum computer and computing integral transformations on a classical computer.

We tested the oo-upCCD VQE approach on the bond dissociation pathways for LiH, H<sub>2</sub>O, and Li<sub>2</sub>O molecule on both quantum simulators and IonQ’s Harmony and Aria quantum computers. We find that on quantum simulators, oo-upCCD gives qualitatively accurate predictions to energy both in the weakly correlated and strongly correlated regime. However, upCCD without orbital optimization produces unphysical behavior in the strongly correlated regime. On quantum hardware, we observed that noisy quantum gate operations yield a consistent positive bias for the energy. Such a consistent bias has also been observed before [26]. In order to understand this, we have performed simulations with both coherent and incoherent noise models on quantum simulators. We find that if the error rate is low enough (below 1%), both error models produce a constant additive error for different molecular geometries, which aligns with the error rate of the Harmony and Aria quantum computers. The simulation results can be found in the supplementary information. Therefore, although the measured absolute energies can be higher than simulator results by hundreds of millihartrees, the relative energies measured are accurate due to the consistency of errors across the PES (i.e., low non-parallelity error).

As with other seniority zero approaches, oo-upCCD proves effective for describing some strong electron correlations but is unable to deliver quantitative accuracy, a difficulty that may in future be addressed in two different ways. First, one may consider implementing the full unitary-CCSD ansatz with quantum circuits, and pay the price of ending up with very deep circuits that are not practical to run on NISQ devices, even with the most efficient compilation techniques. A more practical way is to trade-off circuit depths with measurements and employ approaches such as the quantum subspace expansion (QSE) [37, 53]. QSE will be able to solve two problems at the same time: 1) account for correlations contributed from non-bosonic excitations, and 2) account for correlations contributed from orbitals that are outside of the active space. QSE is able to achieve these two goals without increasing circuit depth, by just performing more measurements to com-

pute higher order RDMs.

In order to achieve quantitative accuracy on a noisy quantum computer using VQE, one would inevitably perform some form of error mitigation. Over the past few years, various error mitigation methods have been developed, such as noise extrapolation [24], density matrix purification [14, 18], symmetry verification [54], randomized compiling [55], and noise-estimation.[56] We believe that an efficient VQE approach combined with measurement based post-processing and noise estimation is a very promising route that harvests the most performance out of near-term quantum computers. Together with continued improvements in quantum hardware, both in terms of qubit number and qubit quality, we will soon see quantum simulation of molecules and materials that surpasses the best classical supercomputers.

## IV. METHODS

### A. Trapped-Ion Quantum Computer

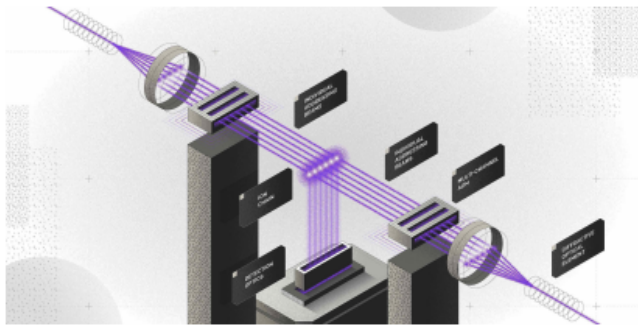


FIG. 7: Schematic of the IonQ Aria quantum computer, where two fans of individually addressable beams illuminate a chain of individually imaged ions.

The experimental demonstration was performed on two generations of quantum processing units (QPU) from IonQ: Harmony and Aria. Both QPUs utilize trapped Ytterbium ions where two states in the ground hyperfine manifold are used as qubit states. These states are manipulated by illuminating individual ions with pulses of 355 nm light that drive Raman transitions between the ground states defining the qubit. By configuring these pulses, arbitrary single qubit gates and Mølmer-Sørensen type two-qubit gates can both be realized. The IonQ Aria QPU (schematic in Figure 7) features not only an order of magnitude better performance in terms of fidelity but also is considerably more robust compared to the IonQ Harmony QPU [57].

### B. upCCD Circuit Design

From the electron pair excitation operators, we can define the pair creation and annihilation operators

$$\begin{aligned} d_a^\dagger &= a_{a\alpha}^\dagger a_{a\beta}^\dagger \\ d_i &= a_{i\beta} a_{i\alpha} \end{aligned} \tag{5}$$

in which  $a_i$  and  $a_i^\dagger$  are the fermionic annihilation and creation operators on orbital  $i$ .  $\alpha$  and  $\beta$  indicate spin up and spin down.

They follow bosonic symmetries

$$\begin{aligned} [d_a^\dagger, d_i] &= 0 \\ [d_i, d_j] &= [d_a^\dagger, d_b^\dagger] = 0 \end{aligned} \quad (6)$$

By performing the Jordan-Wigner Transformation (JWT) to map molecular orbitals to qubits, the pair creation and annihilation operators becomes

$$\begin{aligned} d_a^\dagger &\rightarrow \frac{1}{2}(X_a - iY_a) \\ d_i &\rightarrow \frac{1}{2}(X_i + iY_i) \end{aligned} \quad (7)$$

The pair-excitation operator becomes

$$d_a^\dagger d_i \rightarrow \frac{1}{4}(X_a X_i + iX_a Y_i - iY_a X_i + Y_a Y_i) \quad (8)$$

As one can see from the above equation, after JWT, the pair excitation operator does not have the Pauli-Z strings that occur in general double excitations, due to its bosonic nature.

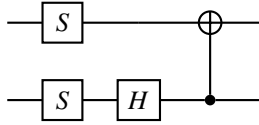
The exponential of the pair-excitation operator, subtracted by its complex conjugate, becomes

$$\begin{aligned} &\exp\left(t_i^a (d_a^\dagger d_i - d_i^\dagger d_a)\right) \\ &= \exp\left(\frac{it_i^a}{2}(X_a Y_i - Y_a X_i)\right). \end{aligned} \quad (9)$$

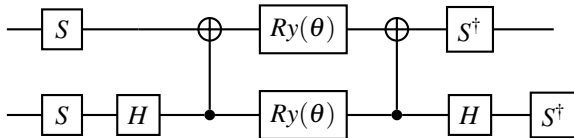
One can then show that this is the Givens rotation matrix

$$\begin{pmatrix} 1 & 0 & 0 & 0 \\ 0 & \cos(\frac{t_i^a}{2}) & -\sin(\frac{t_i^a}{2}) & 0 \\ 0 & \sin(\frac{t_i^a}{2}) & \cos(\frac{t_i^a}{2}) & 0 \\ 0 & 0 & 0 & 1 \end{pmatrix} \quad (10)$$

As has been shown before [27], the Givens rotation matrix belongs to the  $\mathbf{SO}(4)$  group, which can be implemented in 12 elementary (i.e.  $R_y, R_z$ ) gates and 2  $CX$  gates using the magic gate basis



The efficient Givens rotation implementation with angle  $\theta$  is the following circuit.



in which only two  $CX$  gates are required.

### C. Hamiltonian and Energy Measurements

Since the upCCD ansatz conserves electron pairs, the terms in the *ab initio* Hamiltonian that break electron pairs do not contribute to energy. After removing these terms, the Hamiltonian can be written as

$$H = H_1(n_p) + H_2(d_p^\dagger d_q) \quad (11)$$

in which the first term only depends on the number operator

$$n_p = a_p^\dagger a_p \rightarrow \frac{1}{2}(1 - Z_p), \quad (12)$$

and so it can be measured in the computational basis.

The second term only depends on the pair excitation operator defined in Equation 8. Furthermore, we note that the two middle terms in it are associated with purely imaginary coefficients, which do not contribute to energy, so that this term can be measured with all qubits in either the  $X$  or  $Y$  basis. In summary, only 3 circuits are needed to be run in order to measure the energy expectation value for the upCCD ansatz, compared with a number of measurements that scales as  $O(N^4)$  (where  $N$  is the number of orbitals) if no symmetry is exploited, independent of the size of the system. This makes the upCCD ansatz extremely efficient in terms of number of measurements.

### D. Orbital Optimization based on Measurements

The orbital optimization effects can be performed classically with integral transformation. Consider the energy expectation value of the oo-upCCD ansatz.

$$E = \langle \Psi_{\text{upCCD}} | e^{-K} H e^K | \Psi_{\text{upCCD}} \rangle \quad (13)$$

where  $K$  is an anti-Hermitian operator defined in Equation 4. We first organize the elements of the lower triangle of  $K$  into the length- $d$  vector  $\vec{\kappa}$ , where

$$d = (n_o + n_v)(n_o + n_v - 1)/2 \quad (14)$$

Starting from initial orbitals ( $\vec{\kappa} = 0$ ), we expand the energy out to second order in  $\vec{\kappa}$  to obtain

$$E(\vec{\kappa}) \approx E(0) + \vec{\kappa}^T \vec{\omega} + \frac{1}{2} \vec{\kappa}^T Q \vec{\kappa} \quad (15)$$

where the length- $d$  energy gradient  $\vec{\omega}$  and the  $d \times d$  energy Hessian  $Q$  are given by

$$\begin{aligned} \omega_x &= \frac{\partial E(\vec{\kappa})}{\partial \kappa_x} \\ Q_{xy} &= \frac{\partial^2 E(\vec{\kappa})}{\partial \kappa_x \partial \kappa_y} \end{aligned} \quad (16)$$

which in turn are functions of the spinless one- and two-electron reduced density matrices (RDM)

$$\begin{aligned} \gamma_{pq} &= \langle \Psi | a_{p\alpha}^\dagger a_{q\alpha} + a_{p\beta}^\dagger a_{q\beta} | \Psi \rangle \\ \Gamma_{pr}^{qs} &= \langle \Psi | \frac{1}{2} a_{p\alpha}^\dagger a_{q\alpha} a_{r\alpha}^\dagger a_{s\alpha} + \frac{1}{2} a_{p\beta}^\dagger a_{q\beta} a_{r\beta}^\dagger a_{s\beta} \\ &\quad + a_{p\alpha}^\dagger a_{q\alpha} a_{r\beta}^\dagger a_{s\beta} | \Psi \rangle \end{aligned} \quad (17)$$



Since the spinless RDMs are in the form of expectation values, they can be measured on the quantum computer, and since we only need 1- and 2-RDMs, the cost for measuring them is the same as measuring the energy. Using  $\vec{\omega}$  and  $Q$ , we can choose a  $\vec{\kappa}$  that reduces the energy using the Newton-Raphson (NR) method,

$$\vec{\kappa} = -Q^{-1}\vec{\omega} \quad (18)$$

At this point, if we continue with more NR steps until the energy is minimized, we need to implement  $\exp(K)$  using quantum circuits, which increases the circuit depth. However, we can instead reset  $\vec{\kappa}$  to zero by absorbing its effects into one- and two-electron integrals through standard molecular orbital transformation. At this point, another NR step can be taken, and the method can be iterated to convergence. In this way, since  $\vec{\kappa}$  is always zero, we do not need to implement it with quantum circuits. The VQE algorithm is shown in Algorithm 1, and the detailed expressions for the orbital gradients and Hessians in terms of 1- and 2-RDMs, as well as an example of VQE convergence with respect to optimization iterations, can be found in the supplementary information.

---

**Algorithm 1:** VQE Algorithm for oo-upCCD

---

```

while Energy not converged do
  Optimize  $T$  using SPSA
  Update circuit parameters based on the optimal  $T^*$ 
  Optimize  $K$  using NR
  Update orbital parameters based on the optimal  $K^*$ 
  Rotate one- and two-electron integrals to the new orbital
  basis
  Set  $K$  to be 0
  Compute energy to check convergence
end

```

---

## V. DATA AVAILABILITY

The data presented in this manuscript are available from the corresponding author upon reasonable request.

## ACKNOWLEDGMENTS

We thank the Hyundai Motor Company for funding this research through the Hyundai-IonQ Joint Quantum Computing Research Project. We thank Dr. Tae Won Lim and Dr. Seung Hyun Hong for enlightening discussions.

- [1] N. S. Blunt, J. Camps, O. Crawford, R. Izsák, S. Leontica, A. Mirani, A. E. Moylett, S. A. Scivier, C. Sünderhauf, P. Schopf, J. M. Taylor, and N. Holzmann, "A Perspective on the Current State-of-the-Art of Quantum Computing for Drug Discovery Applications," arXiv preprint, arXiv:2206.00551v1 (2022).
- [2] V. von Burg, G. H. Low, T. Häner, D. S. Steiger, M. Reiher, M. Roetteler, and M. Troyer, "Quantum Computing Enhanced Computational Catalysis," *Phys. Rev. Research* **3**, 033055 (2021).
- [3] J. E. Rice, T. P. Gujarati, M. Motta, T. Y. Takeshita, E. Lee, J. A. Latone, and J. M. Garcia, "Quantum Computation of Dominant Products in Lithium–Sulfur Batteries," *J. Chem. Phys.* **154**, 134115 (2021).
- [4] Robert G. Parr and Weitao Yang, *Density-functional theory of atoms and molecules* (Oxford University Press, New York, 1989).
- [5] Attila Szabo and Neil S. Ostlund, *Modern Quantum Chemistry: Introduction to Advanced Electronic Structure Theory* (Dover Publications, Mineola, N.Y., 1996).
- [6] U. Schollwöck, "The density-matrix renormalization group," *Rev. Mod. Phys.* **77**, 259–315 (2005).
- [7] P. R. C. Kent et al, "Qmcpack: Advances in the development, efficiency, and application of auxiliary field and real-space variational and diffusion quantum monte carlo," *J. Chem. Phys.* **152**, 174105 (2020).
- [8] M. A. Nielsen and I. L. Chuang, *Quantum Computation and Quantum Information* (Cambridge University Press, Cambridge, 2010).
- [9] F. Arute, K. Arya, R. Babbush, D. Bacon, J. C. Bardin, and et al, "Quantum Supremacy Using a Programmable Superconducting Processor," *Nature* **574**, 505 (2019).
- [10] Y. Cao, J. Romero, J. P. Olson, M. Degroote, P. D. Johnson, M. Kieferová, L. D. Kivlichan, T. Menke, B. Peropadre, N. P. D. Sawaya, S. Sim, L. Veis, and A. Aspuru-Guzik, "Quantum chemistry in the age of quantum computing," *Chem. Rev.* **119**, 10856–10915 (2019).
- [11] A. Peruzzo, J. McClean, P. Shadbolt, M-H. Yung, X-Q. Zhou, P. J. Love, A. Aspuru-Guzik, and J. O'Brien, "A variational eigenvalue solver on a photonic quantum processor," *Nat. Commun.* **5**, 5213 (2014).
- [12] P. J. J. O'Malley et al, "Scalable quantum simulation of molecular energies," *Phys. Rev. X* **6**, 031007 (2016).
- [13] A. Kandala, A. Mezzacapo, K. Temme, M. Takita, M. Brink, J. M. Chow, and J. M. Gambetta, "Hardware-efficient variational quantum eigensolver for small molecules and quantum magnets," *Nature* **549**, 242–246 (2017).
- [14] Google AI Quantum and Collaborators, "Hartree-Fock on a Superconducting Qubit Quantum Computer," *Science* **369**, 1084–1089 (2020).
- [15] Y. Nam, J-S. Chen, N. C. Pseni, K. Wright, C. Delaney, D. Maslov, K. R. Brown, S. Allen, J. M. Amini, J. Apisdorf, K. M. Beck, A. Blinov, V. Chaplin, M. Chmielewski, C. Collins, S. Debnath, K. M. Hudek, A. M. Ducore, M. Keesan, S. M. Kreikemeier, J. Mizrahi, P. Solomon, M. Williams, J. D. Wong-Campos, D. Moehring, C. Monroe, and J. Kim, "Ground-State Energy Estimation of the Water Molecule on a Trapped-Ion Quantum Computer," *npj Quantum Information* **6**, 33 (2020).
- [16] H. R. Grimsley, D. Claudino, S. E. Economou, E. Barnes, and N. J. Mayhall, "Is the Trotterized UCCSD Ansatz Chemically Well-Defined?" *J. Chem. Theory Comput.* **16**, 1–6 (2020).
- [17] H. R. Grimsley, S. E. Economou, E. Barnes, and N. J. Mayhall, "An Adaptive Variational Algorithm for Exact Molecular Simulations on a Quantum Computer," *Nat. Commun.* **10**, 3007 (2019).
- [18] A. J. McCaskey, Z. P. Parks, J. Jakowski, S. V. Moore, T. D. Morris, T. S. Humble, and R. C. Pooser, "Quantum Chemistry as a Benchmark for Near-Term Quantum Computers," *npj Quantum Information* **5**, 99 (2019).
- [19] A. Cowtan, W. Simmons, and R. Duncan, "A Generic Compilation Strategy for the Unitary Coupled Cluster Ansatz," arXiv preprint, arXiv:2007.10515v3 (2020).
- [20] P. Kl. Barkoutsos, J. F. Gonthier, I. Sokolov, N. Moll, G. Salis, A. Fuhrer, M. Ganzhorn, D. J. Egger, M. Troyer, A. Mezzacapo, S. Filipp, and I. Tavernelli, "Quantum Algorithms for Electronic Structure Calculations: Particle-Hole Hamiltonian and Optimized Wave-Function Expansions," *Phys. Rev. A* **98**, 022322 (2018).
- [21] I. G. Ryabinkin, T-C. Yen, S. N. Genin, and A. F. Izmaylov, "Qubit Coupled Cluster Method: A Systematic Approach to Quantum Chemistry on a Quantum Computer," *J. Chem. Theory Comput.* **14**, 6317–6326 (2018).
- [22] I. G. Ryabinkin, R. A. Lang, S. N. Genin, and A. F. Izmaylov, "Iterative Qubit Coupled Cluster Approach with Efficient Screening of Generators," *J. Chem. Theory Comput.* **16**, 1055–1063 (2020).
- [23] G-L. R. Anselmetti, D. Wierichs, C. Gogolin, and R. M. Parrish, "Local, Expressive, Quantum-Number-Preserving VQE ansätze for Fermionic Systems," *New J. Phys.* **23**, 113010 (2021).
- [24] A. Kandala, K. Temme, A. D. Córcoles, A. Mezzacapo, J. M. Chow, and J. M. Gambetta, "Error Mitigation Extends the Computational Reach of a Noisy Quantum Processor," *Nature* **567**, 491–495 (2019).
- [25] Q. Gao, G. O. Jones, M. Motta, M. Sugawara, H. C. Watanabe, T. Kobayashi, E. Watanabe, Y. Ohnishi, H. Nakamura, and N. Yamamoto, "Applications of Quantum Computing for Investigations of Electronic Transitions in Phenylsulfonfyl-carbazole TADF Emitters," *npj Quantum Information* **7**, 70 (2021).
- [26] T. E. O'Brien and et al, "Purification-based Quantum Error Mitigation of Pair-Correlated Electron Simulations," arXiv preprint, 2210.10799v1 (2022).
- [27] F. Vatan and C. Williams, "Optimal Quantum Circuits for General Two-Qubit Gates," *Phys. Rev. A* **69**, 032315 (2004).
- [28] V. E. Elfving, M. Milaruelo, J. A. Gámez, and C. Gogolin, "Simulating Quantum Chemistry in the Seniority-Zero Space on Qubit-based Quantum Computers," *Phys. Rev. A* **103**, 032605 (2021).
- [29] IT Khan, M Tudorovskaya, JJM Kirsopp, D Muñoz Ramo, PW Warriar, DK Papanastasiou, and R Singh, "Chemically aware unitary coupled cluster with ab initio calculations on system model h1: A refrigerant chemicals application," arXiv preprint arXiv:2210.14834 (2022).
- [30] Josh JM Kirsopp, Cono Di Paola, David Zsolt Manrique, Michal Krompiec, Gabriel Greene-Diniz, Wolfgang Guba, Agnes Meyder, Detlef Wolf, Martin Strahm, and David Muñoz Ramo, "Quantum computational quantification of protein–ligand interactions," *International Journal of Quantum Chemistry* **122**, e26975 (2022).
- [31] Kentaro Yamamoto, David Zsolt Manrique, Irfan T Khan, Hideaki Sawada, and David Muñoz Ramo, "Quantum hardware calculations of periodic systems with partition-

- measurement symmetry verification: Simplified models of hydrogen chain and iron crystals,” *Physical Review Research* **4**, 033110 (2022).
- [32] Mario Motta, Gavin O Jones, Julia E Rice, Tanvi P Gujarati, Rei Sakuma, Ieva Liepuoniute, Jeannette M Garcia, and Yu-ya Ohnishi, “Quantum chemistry simulation of ground-and excited-state properties of the sulfonium cation on a superconducting quantum processor,” arXiv preprint arXiv:2208.02414 (2022).
- [33] Andrew Eddins, Mario Motta, Tanvi P Gujarati, Sergey Bravyi, Antonio Mezzacapo, Charles Hadfield, and Sarah Sheldon, “Doubling the size of quantum simulators by entanglement forging,” *PRX Quantum* **3**, 010309 (2022).
- [34] Y. Kawashima, E. Lloyd, M. P. Coons, Y. Nam, S. Matsuura, A. J. Garza, S. Johri, L. Huntington, V. Senicourt, A. O. Maksymov, J. H. V. Nguyen, J. Kim, N. Alidoust, A. Zaribafiyani, and T. Yamazaki, “Optimizing Electronic Structure Simulations on a Trapped-Ion Quantum Computer using Problem Decomposition,” *Communications Physics* **4**, 245 (2021).
- [35] Qi Gao, Hajime Nakamura, Tanvi P Gujarati, Gavin O Jones, Julia E Rice, Stephen P Wood, Marco Pistoia, Jeannette M Garcia, and Naoki Yamamoto, “Computational investigations of the lithium superoxide dimer rearrangement on noisy quantum devices,” *The Journal of Physical Chemistry A* **125**, 1827–1836 (2021).
- [36] Alexander J McCaskey, Zachary P Parks, Jacek Jakowski, Shirley V Moore, Titus D Morris, Travis S Humble, and Raphael C Pooser, “Quantum chemistry as a benchmark for near-term quantum computers,” *npj Quantum Information* **5**, 1–8 (2019).
- [37] J. I. Colless, V. V. Ramasesh, D. Dahlen, M. S. Blok, M. E. Kimchi-Schwartz, J. R. McClean, J. Carter, W. A. de Jong, and I. Siddiqi, “Computation of Molecular Spectra on a Quantum Processor with an Error-Resilient Algorithm,” *Phys. Rev. X* **8**, 011021 (2018).
- [38] Alberto Peruzzo, Jarrod McClean, Peter Shadbolt, Man-Hong Yung, Xiao-Qi Zhou, Peter J Love, Alán Aspuru-Guzik, and Jeremy L O’Brien, “A variational eigenvalue solver on a photonic quantum processor,” *Nature communications* **5**, 1–7 (2014).
- [39] P. A. Limacher, T. D. Kim, P. W. Ayers, P. A. Johnson, S. D. Baerdemacker, D. Van Neck, and P. Bultinck, “The Influence of Orbital Rotation on the Energy of Closed-Shell Wavefunctions,” *Mol. Phys.* **112**, 853–862 (2014).
- [40] T. M. Henderson, I. W. Bulik, and G. E. Scuseria, “Pair Extended Coupled Cluster Doubles,” *J. Chem. Phys.* **142**, 214116 (2015).
- [41] L. Zhao and E. Neuscamman, “Amplitude Determinant Coupled Cluster with Pairwise Doubles,” *J. Chem. Theory Comput.* **12**, 5841–5850 (2016).
- [42] I. O. Sokolov, P. KI. Barkoutsos, P. J. Ollitrault, D. Greenberg, J. Rice, M. Pistoia, and I. Tavernelli, “Quantum Orbital-Optimized Unitary Coupled Cluster Methods in the Strongly Correlated Regime: Can Quantum Algorithms Outperform Their Classical Equivalents?” *J. Chem. Phys.* **152**, 124107 (2020).
- [43] Qiming Sun, Timothy C Berkelbach, Nick S Blunt, George H Booth, Sheng Guo, Zhendong Li, Junzi Liu, James D McClain, Elvira R Sayfutyarova, Sandeep Sharma, Sebastian Wouters, and Garnet Kin-Lic Chan, “Pyscf: the python-based simulations of chemistry framework,” *Wiley Interdisciplinary Reviews: Computational Molecular Science* **8**, e1340 (2018).
- [44] S. Johri, S. Debnath, A. Mocherla, A. Singk, A. Prakash, J. Kim, and I. Kerenidis, “Nearest Centroid Classification on a Trapped Ion Quantum Computer,” *npj Quantum Information* **7**, 122 (2021).
- [45] M. S. Rudolph, N. B. Toussaint, A. Katarbarwa, S. Johri, B. Peropadre, and A. Perdomo-Ortiz, “Generation of High-Resolution Handwritten Digits with an Ion-Trap Quantum Computer,” *Phys. Rev. X* **12**, 031010 (2022).
- [46] E. Y. Zhu, S. Johri, D. Bacon, M. Esencan, J. Kim, M. Muir, N. Murgai, J. Nguyen, N. Pseni, A. Schouela, K. Sosnova, and K. Wright, “Generative Quantum Learning of Joint Probability Distribution Functions,” arXiv preprint, 2109.06315v1 (2021).
- [47] T. Giurgica-Tiron, S. Johri, I. Kerenidis, J. Nyugen, N. Pseni, A. Prakash, K. Sosnova, K. Wright, and W. Zeng, “Low-depth Amplitude Estimation on a Trapped-Ion Quantum Computer,” *Phys. Rev. Research* **4**, 033034 (2022).
- [48] A. Aspuru-Guzik, A. D. Dutoi, P. J. Love, and M. Head-Gordon, “Simulated quantum computation of molecular energies,” *Science* **309**, 1704–1707 (2005).
- [49] B. P. Lanyon, J. D. Whitfield, G. G. Gillett, M. E. Goggin, M. P. Almeida, I. Kassal, J. D. Biamonte, M. Mohseni, B. J. Powell, M. Barbieri, A. Aspuru-Guzik, and A. G. White, “Towards quantum chemistry on a quantum computer,” *Nat. Chem.* **2**, 106–111 (2010).
- [50] R. Babbush, C. Gidney, D. W. Berry, N. Wiebe, J. McClean, A. Paler, A. Fowler, and H. Neven, “Encoding Electronic Spectra in Quantum Circuits with Linear T Complexity,” *Phys. Rev. X* **8**, 041015 (2018).
- [51] G. H. low and I. L. Chuang, “Hamiltonian Simulation by Qubitization,” *Quantum* **3**, 163 (2019).
- [52] J. Lee, D. W. Berry, C. Gidney, W. J. Huggins, J. R. McClean, N. Wiebe, and R. Babbush, “Even More Efficient Quantum Computations of Chemistry Through Tensor Hypercontraction,” *PRX Quantum* **2**, 030305 (2021).
- [53] T. Takeshita, N. C. Rubin, Z. Jiang, E. Lee, R. Babbush, and J. R. McClean, “Increasing the Representation Accuracy of Quantum Simulations of Chemistry without Extra Quantum Resources,” *Phys. Rev. X* **10**, 011004 (2020).
- [54] S. McArdle, X. Yuan, and S. Benjamin, “Error-Mitigated Digital Quantum Simulation,” *Phys. Rev. Lett.* **122**, 180501 (2019).
- [55] A. Hashim, R. K. Naik, A. Morvan, J-L. Ville, B. Mitchell, J. M. Kreikebaum, M. Davis, E. Smith, C. Iancu, K. P. O’Brien, I. Hincks, J. J. Wallman, J. Emerson, and Irfan Siddiqi, “Randomized Compiling for Scalable Quantum Computing on a Noisy Superconducting Quantum Processor,” *Phys. Rev. X* **11**, 041039 (2021).
- [56] M. Urbaneck, B. Nachman, V. R. Pascuzzi, A. He, C. W. Bauer, and W. A. de Jong, “Mitigating Depolarizing Noise on Quantum Computers with Noise-Estimation Circuits,” *Phys. Rev. Lett.* **127**, 270502 (2021).
- [57] T. Lubinski, S. Johri, P. Varosy, J. Coleman, L. Zhao, J. Necaie, C. H. Baldwin, K. Mayer, and T. Proctor, “Application-oriented performance benchmarks for quantum computing,” arXiv preprint, arXiv:2010.03137v1 (2021).

# Supplementary Information: Orbital-optimized pair-correlated electron simulations on trapped-ion quantum computers

Luning Zhao,\* Joshua Goings, Kenneth Wright, Jason Nguyen, Jungsang Kim, and Sonika Johri  
*IonQ Inc, College Park, MD, 20740, USA*

Kyujin Shin† and Woomin Kyoung  
*Materials Research & Engineering Center, R&D Division,  
Hyundai Motor Company, Uiwang 16082, Republic of Korea*

Johanna I. Fuks  
*Qunova Computing, Daejeon, 34051, Republic of Korea*

June-Koo Kevin Rhee  
*Qunova Computing, Daejeon, 34051, Republic of Korea and  
School of Electrical Engineering, KAIST, Daejeon, 34141, Republic of Korea*

Young Min Rhee  
*Department of Chemistry, KAIST, Daejeon, 34141, Republic of Korea*  
(Dated: December 6, 2022)

## S1. EXPERIMENTAL METHODS

### A. Single-qubit operation

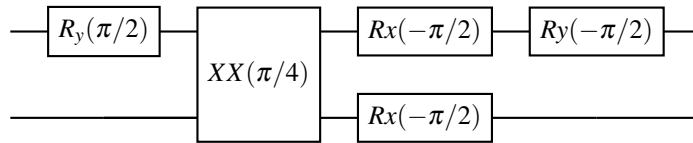
Single-qubit gates are implemented via Rabi oscillations between  $|0\rangle$  and  $|1\rangle$ , using an SK1 composite pulse sequence. The transition is driven by a two-photon Raman process from two separate beams generated by a pulsed 355 nm laser, where one beam is tightly focused onto the ion so it can be manipulated independently from the rest of the chain. We prepare arbitrary single-qubit states on the Bloch sphere by controlling the phase and pulse area delivered by the individual addressing beam. Conventional randomized benchmarking and gate set tomography techniques are used to characterize our single-qubit gates, and we observe fidelities 99% for Harmony and 99.94% for Aria with good repeatability.

### B. Two-qubit operation

Two-qubit entangling gates are implemented via the Mølmer-Sørensen interaction, where an amplitude-modulated laser pulse, composed of non-copropagating beams, achieves full spin-motion decoupling at the end of the gate. One of the laser beams uniformly illuminates the ions, while the other individually addresses the two particular ions involved in the gate. By varying the pulse area through the laser intensities, we control the geometric phase  $\theta$  of the interaction, defined in terms of the Pauli-X matrices  $X_i$  on the  $i$ th ion as

$$XX_{ij}(\theta) = e^{-i\theta X_i X_j} \quad (\text{S1})$$

We calibrate the the maximally entangling  $XX$  gate with  $\theta = \pi/4$ , and  $CX$  gates are implemented as



in which 1  $XX$  gates are needed.

\* zhao@ionq.co

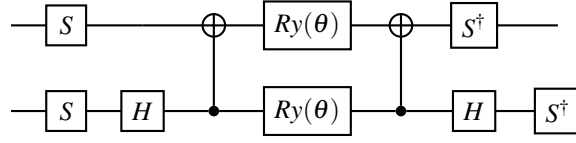
† shinkj@hyundai.com

## C. IonQ Harmony and Aria

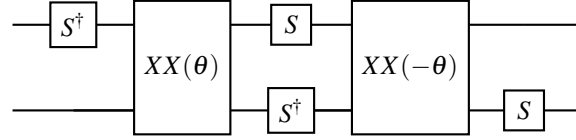
### S2. THEORY METHODS

#### A. Comparison of Two Implementations of the Givens Rotation

In the main text, the Givens rotation is implemented as



Besides using the magic gate basis, another way of implementing the Givens rotation is to use the  $R_{xx}$  gates using the following circuit,



in which two  $R_{xx}$  gates are used.

The above circuit is more efficient than the circuit using magic gate basis on trapped-ion quantum computers since the  $XX$ -Ising interactions are native. However, this requires calibration of arbitrary angle  $R_{xx}$  gates on the hardware level, as was done in IonQ's previous study [? ]. On IonQ's Harmony and Aria quantum computers, only the  $R_{xx}$  gate with a fixed angle ( $\pi/4$ ) is calibrated, and any arbitrary angle  $R_{xx}$  gate will be compiled to 2  $CX$  gates first, then further transpiled to 4 fixed angle  $R_{xx}$  gates, which results in two times more entangling gates operations than the circuit using magic gate basis. This makes the latter circuit more efficient.

#### B. Expectation values of the Hamiltonian

In order to measure the energy of the upCCD ansatz on the quantum computer, we first write the *ab initio* Hamiltonian as

$$\begin{aligned}
 H = & \sum_{pq} g_{pq} \left( a_{p\alpha}^\dagger a_{q\alpha} + a_{p\beta}^\dagger a_{q\beta} \right) \\
 & + \sum_{pqrs} (pq|rs) \left( \frac{1}{2} a_{p\alpha}^\dagger a_{q\alpha} a_{r\alpha}^\dagger a_{s\alpha} + \frac{1}{2} a_{p\beta}^\dagger a_{q\beta} a_{r\beta}^\dagger a_{s\beta} \right) \\
 & + \sum_{pqrs} (pq|rs) a_{p\alpha}^\dagger a_{q\alpha} a_{r\beta}^\dagger a_{s\beta}
 \end{aligned} \tag{S2}$$

in which  $(pq|rs)$  is the usual two-electron coulomb integrals in (11|22) order, and  $g_{pq}$  are modified one-electron integral

$$g_{pq} = h_{pq} - \frac{1}{2} \sum_r (pr|rq) \tag{S3}$$

For the upCCD wave function, only a subset of the Hamiltonian terms will contribute to the energy. The first part involves only number operators

$$\begin{aligned}
 H_1 = & \sum_p g_{pp} (n_{p\alpha} + n_{p\beta}) \\
 & + \sum_{pq} (pp|qq) \left( \frac{1}{2} n_{p\alpha} n_{q\alpha} + \frac{1}{2} n_{p\beta} n_{q\beta} + n_{p\alpha} n_{q\beta} \right) \\
 & + \sum_{p \neq q} (pq|qp) \left( \frac{1}{2} n_{p\alpha} (1 - n_{q\alpha}) + \frac{1}{2} n_{p\beta} (1 - n_{q\beta}) \right)
 \end{aligned} \tag{S4}$$

and an additional term

$$H_2 = \sum_{p \neq q} (pq|pq) a_{p\alpha}^\dagger a_{q\alpha} a_{p\beta}^\dagger a_{q\beta} \quad (\text{S5})$$

For the first part of the Hamiltonian, we need to compute the following expectation values

$$\begin{aligned} z_p &= \langle n_{p\alpha} + n_{p\beta} \rangle \\ \Gamma_{pq} &= \langle n_{p\alpha} n_{q\alpha} + n_{p\beta} n_{q\beta} \rangle \\ \Delta_{pq} &= \langle n_{p\alpha} n_{q\beta} \rangle. \end{aligned} \quad (\text{S6})$$

For the first one, one can measure the  $p$ th qubit in the  $Z$  basis, and multiply the measured results by 2. For the second term, one can measure both the  $p$ th and the  $q$ th qubit in the  $Z$  basis, and if both measurements give 1, this term is 2, otherwise this term is 0. For the third term, we also measure the  $p$ th and the  $q$ th qubit, and if both measurements give 1, this term is 1, and 0 otherwise.

Then the simple part of the Hamiltonian becomes

$$\begin{aligned} \langle H_1 \rangle &= \sum_p g_{pp} z_p + \sum_{pq} (pp|qq) \left( \frac{1}{2} \Gamma_{pq} + \Delta_{pq} \right) \\ &+ \sum_{p \neq q} \frac{1}{2} (pq|qp) (z_p - \Gamma_{pq}) \end{aligned} \quad (\text{S7})$$

For  $H_2$ , we first re-arrange terms

$$\begin{aligned} H_2 &= \sum_{p \neq q} (pq|pq) a_{p\alpha}^\dagger a_{q\alpha} a_{p\beta}^\dagger a_{q\beta} \\ &= - \sum_{p \neq q} (pq|pq) a_{p\alpha}^\dagger a_{p\beta}^\dagger a_{q\alpha} a_{q\beta} \\ &= \sum_{p \neq q} (pq|pq) a_{p\alpha}^\dagger a_{p\beta}^\dagger a_{q\beta} a_{q\alpha} \\ &= \sum_{p \neq q} (pq|pq) d_p^\dagger d_q \end{aligned} \quad (\text{S8})$$

which, upon JWT, becomes

$$\begin{aligned} H_2 &= \frac{1}{4} \sum_{p \neq q} (pq|pq) (X_p X_q + i X_p Y_q - i Y_p X_q + Y_p Y_q) \\ &= \frac{1}{2} \sum_{p > q} (pq|pq) (X_p X_q + Y_p Y_q) \end{aligned} \quad (\text{S9})$$

which can be measured by measuring qubit  $p$  and  $q$  and  $X$  or  $Y$  basis.

As one can see, only 3 circuits are needed to be run in order to measure the energy expectation value for the upCCD ansatz, and it does not depend on the size of the system. This makes the upCCD ansatz extremely efficient in terms of number of measurements.

### C. Analytical Expressions for Orbital Gradient and Hessian

For completeness, we include here expressions for the oo-upCCD orbital rotation gradient and hessian. These should provide everything needed for the Newton-Raphson algorithm we use for orbital optimization.

The energy can be written as

$$E(\vec{\kappa}) = \langle \Psi | e^{-\hat{K}} H e^{\hat{K}} | \Psi \rangle \quad (\text{S10})$$

with

$$\hat{K} = \sum_{p > q} \sum_{\sigma} K_{pq} (a_{p\sigma}^\dagger a_{q\sigma} - a_{q\sigma}^\dagger a_{p\sigma}) \quad (\text{S11})$$

where we evaluate the orbital rotation unitary transformation as  $\exp(\hat{K})$  and transform the integrals into this new basis.

The orbital gradient is

$$\begin{aligned}
& \left( \frac{\partial E}{\partial K_{pq}} \right)_{\vec{k}=0} \\
&= \mathcal{P}_{pq} \sum_{\sigma} \langle [H, a_{p\sigma}^{\dagger} a_{q\sigma}] \rangle \\
&= \mathcal{P}_{pq} (g_{up} \gamma_{uq} - g_{qu} \gamma_{pu}) \\
&+ \mathcal{P}_{pq} ((uv|tp) \Gamma_{uv}^{tq} + (up|tv) \Gamma_{uq}^{tv} - (uv|qt) \Gamma_{uv}^{pt} - (qv|tu) \Gamma_{pv}^{tu})
\end{aligned} \tag{S12}$$

where  $\mathcal{P}_{pq}$  is a permutation operator  $\mathcal{P}_{pq} = 1 - (p \leftrightarrow q)$ , and Einstein summation is used.

Similarly, the Hessian is

$$\begin{aligned}
Q_{pq,rs} &= \left( \frac{\partial^2 E}{\partial K_{pq} \partial K_{rs}} \right)_{\vec{k}=0} \\
&= \frac{1}{2} \mathcal{P}_{pq} \mathcal{P}_{rs} \sum_{\sigma, \tau} \langle [[H, a_{p\sigma}^{\dagger} a_{q\sigma}], a_{r\tau}^{\dagger} a_{s\tau}] \rangle \\
&+ \frac{1}{2} \mathcal{P}_{pq} \mathcal{P}_{rs} \sum_{\sigma, \tau} \langle [[H, a_{r\sigma}^{\dagger} a_{s\sigma}], a_{p\tau}^{\dagger} a_{q\tau}] \rangle
\end{aligned} \tag{S13}$$

We obtain

$$\begin{aligned}
Q_{pq,rs} &= -\mathcal{P}_{pq} \mathcal{P}_{rs} (g_{sp} \gamma_{qr} + g_{ps} \gamma_{rq}) \\
&+ \frac{1}{2} \mathcal{P}_{pq} \mathcal{P}_{rs} (\delta_{qr} g_{tp} \gamma_{ts} + \delta_{qr} g_{st} \gamma_{pt} + \delta_{ps} g_{qt} \gamma_{rt} + \delta_{ps} g_{tr} \gamma_{q}) \\
&- \mathcal{P}_{pq} \mathcal{P}_{rs} ((ut|qr) \Gamma_{ut}^{ps} + (qu|tr) \Gamma_{pu}^{ts} + (ur|qt) \Gamma_{us}^{pt} + (qr|tu) \Gamma_{ps}^{tu} \\
&+ (ut|sp) \Gamma_{ut}^{tq} + (up|st) \Gamma_{uq}^{rt} + (su|tp) \Gamma_{ru}^{tq} + (sp|tu) \Gamma_{rq}^{tu}) \\
&+ \mathcal{P}_{pq} \mathcal{P}_{rs} ((up|vr) \Gamma_{uq}^{vs} + (ur|vq) \Gamma_{us}^{vq} + (qv|su) \Gamma_{pv}^{ru} + (sv|qu) \Gamma_{rv}^{ru}) \\
&+ \frac{1}{2} \mathcal{P}_{pq} \mathcal{P}_{rs} (\delta_{qr} (uv|tp) \Gamma_{uv}^{ts} + \delta_{qr} (up|tv) \Gamma_{us}^{tv} + \delta_{qr} (uv|st) \Gamma_{uv}^{pt} \\
&+ \delta_{qr} (sv|tu) \Gamma_{pv}^{tu} + \delta_{ps} (uv|qt) \Gamma_{uv}^{rt} + \delta_{ps} (qv|tu) \Gamma_{rv}^{tu} \\
&+ \delta_{ps} (uv|tr) \Gamma_{uv}^{tq} + \delta_{ps} (ur|tv) \Gamma_{uq}^{tv})
\end{aligned} \tag{S14}$$

in which  $\delta_{pq}$  is 1 if  $p = q$  and 0 otherwise, and Einstein summation is also used.

#### D. Numerical Experimental Details

The upCCD and oo-upCCD circuits are implemented in the Qiskit software platform,[?] and all the simulator results are obtained from the qasm\_simulator provided by Qiskit. The hardware results are obtained from IonQ's Harmony and Aria quantum computers. The full configuration interaction results were obtained from Psi4.[?] The O and Li 1s orbitals are frozen at the RHF level. On Harmony, we take 8192 shots for LiH. On Aria, we take 2000 shots for LiH and H<sub>2</sub>O and 6000 shots for Li<sub>2</sub>O. The simultaneous perturbation stochastic approximation (SPSA) optimization technique is used to optimized the VQE circuit parameters. All the calculations are performed in the STO-3G basis set provided by the PySCF[?] package. The H<sub>2</sub>O bond angle is fixed at 109.57°. Error bars on the potential energy surface plots are due to finite samplings.

#### E. Convergence of VQE

The measured oo-upCCD energy on Aria for Li<sub>2</sub>O as a function of the number of macro iterations that contain optimizations of both  $T$  and  $K$  is shown in Figure S1. As one could see, it converges in about 10 iterations.

#### F. Justification of Energy Shift

In order to justify the constant energy shift we used in the main text, we performed numerical simulations for the upCCD circuit with different noise models. We consider the following two different type of noise channels.

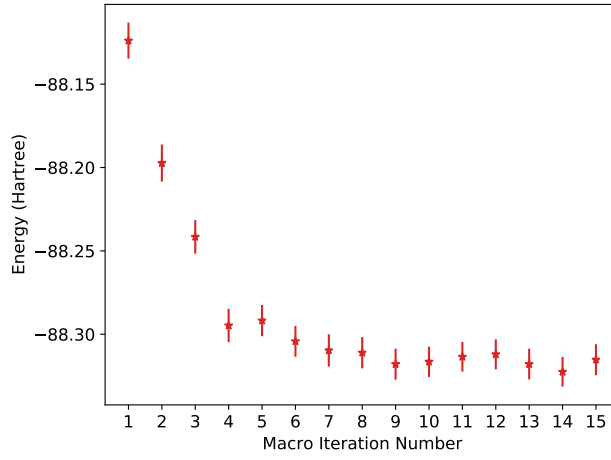
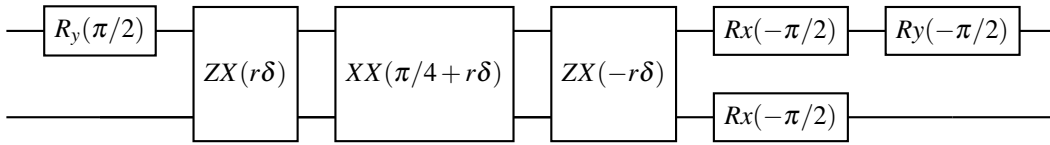


FIG. S1: Convergence of energy for the Li<sub>2</sub>O molecule with  $R = 2.4$  Angstrom with respect to VQE iterations.

### 1. Coherent Noise

Coherent noise is simulated by changing the  $CX$  gate implementation to



in which  $r$  is the error rate, and  $\delta$  is a random variable sampled from  $N(0, 1)$ .

We then use the above  $CX$  implementation to simulate the  $H_2$  molecule in the minimal basis set using the upCCD circuit with the *qasm* simulator. We use 2000 shots and resample  $\delta$  every 10 shots. Two different geometry points are used. The first one is  $R = 0.74$  Angstrom, in which  $R$  is the distance between the two hydrogen atoms, and the second one is  $R = 1.74$  Angstrom. We will refer the first one as equilibrium and the second one as stretched. The simulate energy error v.s. noise-free simulation is shown in Figure S2 .

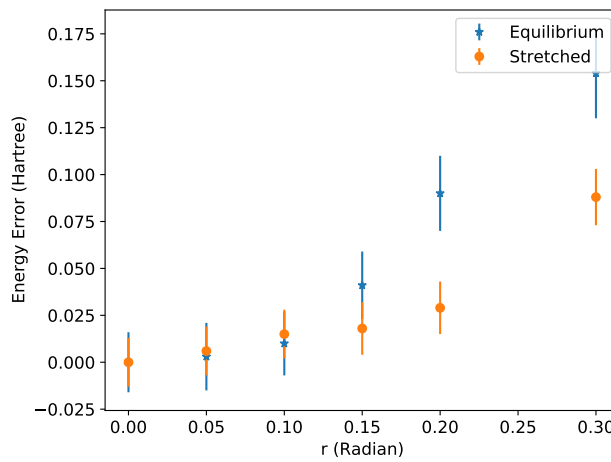


FIG. S2: VQE energy error as a function of  $r$  in the coherent error model.



## 2. Incoherent Noise

Incoherent noise is simulated by using a depolarization noise channel

$$\mathcal{E}(\rho) = (1 - r)\rho + rI/2^N \quad (\text{S15})$$

in which  $\rho$  is the density matrix,  $r$  is the error rate,  $I$  is the identity matrix, and  $N$  is the number of qubits.

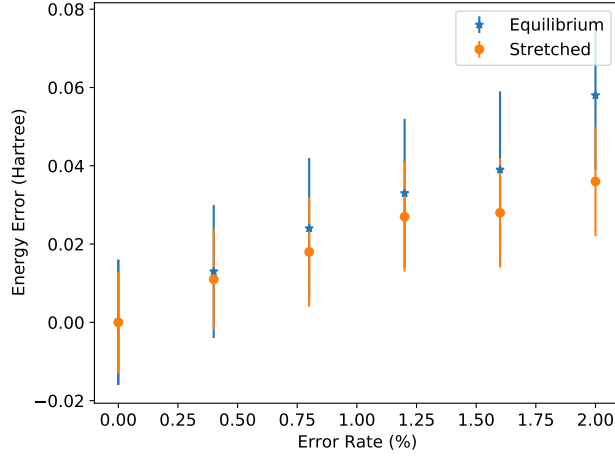


FIG. S3: VQE energy error as a function of error rate in the incoherent error model.

We then use this error channel for  $R_{xx}$  gate in the  $CX$  decomposition to simulate the same systems as in the coherent noise case, and the results are shown in Figure S3.

As we can see from both figures, when the error rate is small enough, the energy errors for the two geometry points are indistinguishable, which justifies the constant shift we used in the main text to correct the VQE experimental energy.